Vibrational Relaxation Completes the Excitation Energy Transfer and Localization of Vibronic Excitons in Allophycocyanin $\alpha_{84} - \beta_{84}$

Ping-Jui Eric Wu[1,2], Siddhartha Sohoni[1,2], Gregory S. Engel[1*]
1. Department of Chemistry, James Franck Institute, The Institute of Biophysical Dynamics, Pritzker School of Molecular Engineering, The University of Chicago, Chicago IL 60637
2. contributed equally

*Corresponding author: gsengel@uchicago.edu

Abstract

The phycobilisome, a light-harvesting complex that plays a key role in photosynthesis in cyanobacteria, generates more than 40% of the world's oxygen. The near-unity excitation energy transfer efficiency from phycobilisomes to photosystems highlights its importance in understanding efficient energy transfer processes. Spectroscopic studies have shown that the 280-fs rapid excitonic downhill energy transfer within the $\alpha_{84} - \beta_{84}$ chromophore dimer in allophycocyanin (APC), a subunit of phycobilisomes, is crucial to this efficiency. However, the role of strong chromophore-protein interactions and vibrational relaxation requires further exploration to fully explain this efficient downhill energy transfer. A theory is required that adequately describes exciton dynamics in an intermediate region while also incorporating vibrational relaxation mediated by protein bath modes. In this work, we incorporate vibrational relaxation into modified Redfield theory by introducing coupling fluctuation. We holistically simulate the rapid excitation energy transfer process of the $\alpha_{84} - \beta_{84}$ chromophore dimer in APC and successfully model the recently observed rapid energy capture. We find that vibrational relaxation dictates excitons captured by the localized state of the β_{84} chromophore. The calculated rate shows excellent agreement with previous ultrafast spectroscopic experiments. Our results show that the inclusion of vibrational relaxation is essential for systems that utilize vibronic coupling to enhance energy transfer and capture. Consequently, vibrational relaxation incorporated Modified Redfield theory shows promise for accurately describing excitation energy transfer process in other photosynthetic systems.

TOC

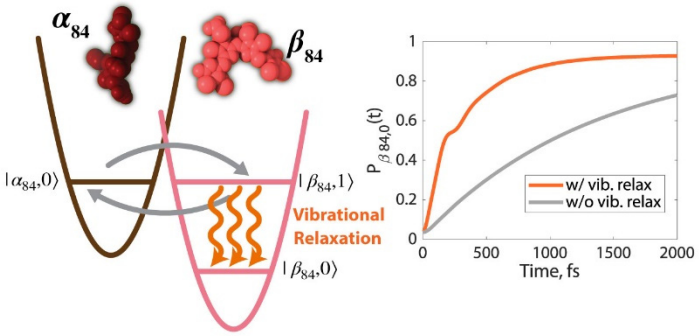

Main text

Excitation energy transfer (EET) is utilized by photosynthetic complexes to harvest sunlight[2, 3]. Excitons travel large distances (~50 nm) in photosynthetic light harvesting antenna complexes[2]. Phycobilisomes (**Figure 1**) are few-MDa light-harvesting antennae in cyanobacteria. Even though they contain around four hundred chromophores, the overall quantum efficiency of the excitation energy transfer from their C-phycocyanin (CPC) rod, into their allophycocyanin (APC) core and eventually into the attached photosystems, is near unity[4, 5]. Many ultrafast spectroscopic[6-12] studies have revealed energy transfer rates between different units of a phycobilisome, and theoretical understandings of these EET processes are desirable.

The Förster resonance energy transfer (FRET) mechanism[12, 13] can describe most of the energy transfer processes in phycobilisomes because the distribution of chromophores in phycobilisomes is sparse. However, in both CPC and APC units of phycobilisomes, a strongly coupled chromophore dimer covalently bonded to the α_{84} and β_{84} polypeptides, the α_{84}-β_{84} chromophore dimer, is separated from each other by only 2 nm[14]. At this distance, the point dipole approximation breaks down. Additionally, anisotropy transient-grating experiments[6, 7, 12] show that the α_{84}-β_{84} chromophore dimers in both CPC and APC exhibit exceptionally fast downhill energy transfer rates of around 500 and 280 fs, respectively. The α_{84}-β_{84} chromophore dimer in APC is particularly interesting because it has a larger site energy difference (760 cm^{-1}) compared to the chromophore dimer in CPC, whose site energy difference is only 200 cm^{-1}, yet it has a faster downhill energy transfer rate. To explain this counterintuitive trend, Womick et al.[15] constructed a vibronic exciton model comprising the dimer system and an 818 cm^{-1} hydrogen-out-of-plane (HOOP) mode and utilized modified Redfield theory to calculate the energy transfer rate. Their results successfully showed that the HOOP mode resonantly enhances the energy transfer rate in the α_{84}-β_{84} chromophore dimer in APC between two near degenerate vibronic exciton states. Nonetheless, the downhill energy transfer process toward the lowest energy state, the localized state of β_{84} chromophore in the vibronic exciton model, was not studied. Besides the transient grating experiment, a fast growing cross-peak was also observed in the photon-echo experiments of Moran and Womick[7]. Recent single-molecule pump-probe experiments by Schlau-Cohen[16] and coworkers demonstrated that the spectral redshift associated with exciton relaxation into the localized lowest-energy β_{84} state also occurs within 200 fs. All these findings drive us to revisit the excitation energy transfer and the energy capture of the α_{84}-β_{84} chromophore dimer in APC. Relaxation into the localized β_{84} state can lead to a significant change in the transition dipole moment and the energy difference, and therefore it is more likely that the relaxation into the localized β_{84} state is the decayed signal observed in the anisotropic experiment, photon-echo experiment, and the recent single-molecule pump probe experiment.

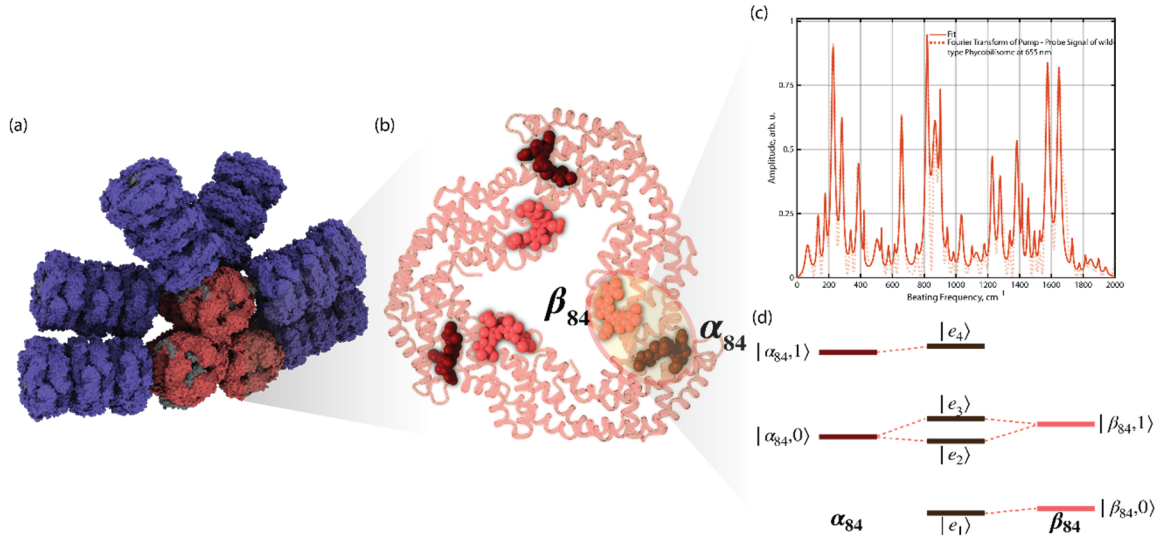

Figure 1: (a) Cryo-EM Structure of *Synechocystis* 6803 phycobilisome[1] with phycocyanin (CPC) in blue and allophycocyanin (APC) in red. (b) Zoom-in of a single disk of APC. Chromophore close to the β_{84} residue is in light red and the one close to α_{84} is in dark red. (c)The spectral density of the α_{84}-β_{84} chromophore dimer in APC extracted from the vibrational coherence signals of the broad-band pump-probe experiment of intact phycobilisomes. (d)Demonstration of vibronic Frenkel exciton formation of a α_{84}-β_{84} chromophore dimer in APC. Light red states are β_{84} site vibronic state with zero and one vibrational quantum of 818 cm^{-1} HOOP mode, dark red states are α_{84} site vibronic state with zero and one vibrational quantum of HOOP mode, and brown states are Frenkel exciton states forming from the superposition of site vibronic states.

To fully model the downhill energy transfer process of the α_{84}-β_{84} chromophore dimer in APC, it is necessary to incorporate the vibrational relaxation effect in a vibronic exciton model[17, 18]. Vibrational relaxation is usually ignored in excitation energy transfer simulations either because vibrational modes are regarded as solely bath degrees of freedom in a Frenkel exciton model or due to the harmonic approximation of vibrational modes. In the harmonic approximation, there is no coupling between states with different vibrational quanta in a vibronic exciton model. Several methods have been proposed to address this shortcoming. For instance, the most common way is to adopt phenomenological relaxation parameters in the Lindblad equation[17] or quantum Langevin equation[19]. In addition, Bennett et al. have offered a vibronic Redfield theory which introduces an additional bath coupling exclusive to vibrational states of the vibronic model in Redfield theory[20]. However, a theory capable of incorporating microscopic bath effects into the energy transfer rate and going beyond the weak system-bath coupling regime, is still desirable. To explicate the effect of vibrational relaxation and study the overall energy capture dynamics of the dimer in APC, we introduce the vibrational relaxation in a vibronic exciton model into the modified Redfield theory[21, 22] (MRT).

MRT has been applied extensively in numerous excitonic systems[23-25] due to its excellent performance in describing exciton dynamics in the intermediate region where the system-bath coupling, and Coulombic coupling are of the same order of magnitude. To incorporate vibrational relaxation of a vibronic excitonic system into MRT, we add a coupling fluctuation term in the system-bath Hamiltonian for the vibrational states on the same monomer site. Without introducing the anharmonicity of a vibrational mode, coupling fluctuation is the only way that the bath degrees of freedom can induce vibrational relaxation. By benchmarking the vibrational relaxation rate to the rate of dynamic Stokes shift from the

photon-echo experiment[7] and the rate of intramolecular vibrational redistribution from a hole-burning detection pump-probe experiment, our vibrational relaxation incorporated MRT successfully yields the rapid downhill energy transfer rate of the α_{84}-β_{84} chromophore dimer in APC, and the obtained rate shows excellent agreement with the experimental observed rate (~ 280 fs)[7, 10]. Our method allows a more complete picture of the energy transfer dynamics of the dimer system in APC. This extended MRT can also be utilized to investigate the relaxation dynamics of other photosynthetic systems or light-harvesting complexes since utilization of protein bath modes to achieve a rapid energy transfer is ubiquitous in nature.

To investigate the effect of the 818 cm^{-1} HOOP mode on the excitation energy transfer dynamics within the α_{84}-β_{84} chromophore dimer in APC, we adopted a vibronic exciton model. The Hamiltonian is:

$$H = H_s + H_b + H_{sb}, \tag{1}$$

$$H_s = \sum_n \sum_{n_v} (\epsilon_n + n_v \hbar\omega_{HOOP}) |n; n_v\rangle\langle n; n_v| + \sum_{n,m} \sum_{n_v,m_v} V_{nm} S_{n,0n_v} S_{m,0m_v} |n; n_v\rangle\langle m; m_v|, \tag{2}$$

$$H_b = \sum_i \hbar\omega_i \left(a_i^+ a_i + \frac{1}{2}\right), \tag{3}$$

$$H_{sb} = \sum_{n,n_v} \sum_i g_{n,i} \hbar\omega_i (a_i^+ + a_i) |n; n_v\rangle\langle n; n_v| . \tag{4}$$

H_s is the system Hamiltonian, and $n, n_v, \epsilon_n, \omega_{HOOP}, V_{nm}$ and $S_{n,0n_v}$ denote the monomer indices, the number of vibrational quanta of the HOOP mode, the site energy of the n^{th} monomer, the frequency of the HOOP mode, the Coulombic coupling between the n^{th} and m^{th} monomer and the Franck-Condon factor between the ground vibrational state and the n_v excited vibrational state of the HOOP mode on the n^{th} monomer, respectively. We write the Hamiltonian in a general way. In our system, there are only two monomers (n=2) and we only considered up to the first vibrational excited states (n_v=1) of the HOOP mode in our system because of the low Huang-Rhys factor of the HOOP mode. In the bath Hamiltonian H_b and system-bath Hamiltonian H_{sb}, $i, \omega_i, a_i^+ (a_i)$ and $g_{n,i}$ stand for the bath mode indices, the frequency of the i^{th} mode, the creation(annihilation) operator of the i^{th} mode, and the system-bath coupling strength between the n^{th} monomer and the i^{th} bath mode, respectively. Note, in the above expression, we assume the coupling strength is the same for HOOP vibrational states on the same monomers, i.e., $g_{(n,n_v),i} = g_{(n,n_v'),i} = g_{ni}$. In a more general case, g_{ni} depends on the vibrational quantum number n_v if the anharmonic effect of the vibrational mode is considered. However, as no pronounced anharmonic effect has been reported for this HOOP mode, we ignore it for simplicity and only label the system-bath coupling strength by their site indices.

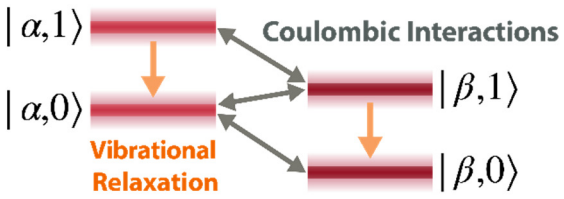

$$H = \begin{bmatrix} \epsilon_\alpha + \delta\epsilon_\alpha & 0 + \delta V & V_{\alpha\beta}S_{\alpha,00}S_{\beta,00} & V_{\alpha\beta}S_{\alpha,00}S_{\beta,01} \\ 0 + \delta V & \epsilon_\alpha + \hbar\omega + \delta\epsilon_\alpha & V_{\alpha\beta}S_{\alpha,01}S_{\beta,00} & V_{\alpha\beta}S_{\alpha,01}S_{\beta,01} \\ V_{\beta\alpha}S_{\alpha,00}S_{\beta,00} & V_{\beta\alpha}S_{\alpha,10}S_{\beta,00} & \epsilon_\beta + \delta\epsilon_\beta & 0 + \delta V \\ V_{\beta\alpha}S_{\alpha,00}S_{\beta,10} & V_{\beta\alpha}S_{\alpha,10}S_{\beta,10} & 0 + \delta V & \epsilon_\beta + \hbar\omega + \delta\epsilon_\beta \end{bmatrix} + H_b$$

Figure 2: A site basis Hamiltonian of a vibronic dimer including coupling fluctuation δV and the diagrammatic representation of the relaxation pathway of a vibronic dimer. We considered up to the first vibrational excited state for vibronic states on both α and β sites and the fluctuation of these states are governed by energy gap fluctuation $\delta\epsilon_k$ for k = α, β. Relaxation of the vibronic dimer can be either through the Coulombic interaction (in gray) or vibrational relaxation (in orange). The amplitude of the Coulombic interaction is determined by coupling $V_{\alpha\beta}$ and the Franck-Condon factor $S_{k,n_v m_v}$ where n_v and m_v stand for vibrational quanta, and vibrational relaxation is caused by coupling fluctuation δV in block diagonals.

So far, the system-bath interaction only allows the bath to affect the diagonal elements of the Hamiltonian. With this Hamiltonian, no transition occurs between states with zero coupling, i.e., vibrational states on a monomer. As a result, there is no vibrational relaxation. To address this issue, we borrowed an idea from vibrational relaxation theory[26, 27], where we introduced the off-diagonal system bath interaction between two vibrational states on the same monomer (n=m and $n_v \neq m_v$) Doing so adds the coupling fluctuation into the model. The derivation for off-diagonal system-bath coupling causing vibrational relaxation is in supporting information. This approach maintains the zero-coupling feature between two vibrational states on the same monomers and thereby keeps the excitonic structure the same while allowing transitions to occur. Combining this with the diagonal system-bath interaction, we obtain a general system-bath Hamiltonian $H_{sb}^{vib-relax}$ which allows the bath to promote vibrational relaxation:

$$H_{sb}^{vib-relax} = \sum_{n,n_v}\sum_{m,m_v}\sum_{i} g_{nn_v,mm_v,i}\hbar\omega_i(a_i^+ + a_i)|n;n_v\rangle\langle m;m_v|\,. \tag{5}$$

To prevent subscripts from becoming cumbersome, we used $|N\rangle$ to represent a vibronic state $|n,n_v\rangle$. In this general system-bath Hamiltonian, $g_{NM,i}$ is the system-bath coupling strength of the ith bath mode to the site energy of the Nth vibronic state if N=M, and the system-bath coupling strength of the ith bath mode to the coupling between the Nth and Mth vibronic states if $N \neq M$.

Incorporating this general system-bath Hamiltonian into modified Redfield theory is quite straightforward because the new Hamiltonian does not change the form of the rate equations, only the meaning of the states represented by the subscripts. Specifically, we follow the same route of deriving modified Redfield rate equation by treating the off-diagonal system-bath coupling in the exciton basis as a perturbation (See supplementary information). With the Markovian approximation and ignoring the

coherence dynamics, the form of the resultant rate equation is identical to the rate equation of the standard modified Redfield theory:

$$R_{\alpha\beta} = 2Re\int_0^\infty d\tau F_\beta^*(\tau)A_\alpha(\tau)X_{\alpha\beta}(\tau)\,, \tag{6}$$

$$F_\beta(t) = e^{-i(\epsilon_\beta - 2\lambda_{\beta\beta\beta\beta})t - g^*_{\beta\beta\beta\beta}(t)}, \tag{7}$$

$$A_\alpha(t) = e^{-i\epsilon_\alpha t - g_{\alpha\alpha\alpha\alpha}(t)}, \tag{8}$$

$$X_{\alpha\beta}(t) = e^{\left(g_{\alpha\alpha\beta\beta}(t)+g_{\beta\beta\alpha\alpha}(t)+i(\lambda_{\alpha\alpha\beta\beta}+\lambda_{\beta\beta\alpha\alpha})t\right)}\big[\ddot{g}_{\beta\alpha\alpha\beta}(t) - \left(\dot{g}_{\beta\alpha\alpha\alpha}(t) - \dot{g}_{\beta\alpha\beta\beta}(t) - 2i\lambda_{\beta\alpha\beta\beta}\right)\times\left(\dot{g}_{\alpha\beta\alpha\alpha}(t) - \dot{g}_{\alpha\beta\beta\beta}(t) - 2i\lambda_{\alpha\beta\beta\beta}\right)\big]. \tag{9}$$

However, the bath-related quantities are now in a more general form. Greek letters are the state indices in the eigenbasis, and $R_{\alpha\beta}$ stands for the energy transfer rate from the excitonic state β to the excitonic state α. In the above equation, we used the eigenbasis lineshape function $g_{\alpha\beta\gamma\delta}(t)$ and eigenbasis reorganization energy $\lambda_{\alpha\beta\gamma\delta}$. These two quantities can be calculated from the transformation by using $C_N^\alpha = \langle N|\alpha\rangle$:

$$g_{\alpha\beta\gamma\delta}(t) = \sum_{NMN'M'} C_N^\alpha C_M^\beta C_{N'}^\gamma C_{M'}^\delta g_{NM,N'M'}(t)\,, \tag{10}$$

$$\lambda_{\alpha\beta\gamma\delta} = \sum_{NMN'M'} C_N^\alpha C_M^\beta C_{N'}^\gamma C_{M'}^\delta \lambda_{NM,N'M'} \tag{11}$$

with the lineshape function and reorganization energy in the site basis:

$$g_{NM,N'M'}(t) = \int_0^\infty d\omega \frac{J_{NM,N'M'}(\omega)}{\omega^2}\left\{\coth\left(\frac{\omega}{2k_BT}\right)[1-\cos\omega t] + i[\sin\omega t - \omega t]\right\}, \tag{12}$$

$$\lambda_{NM,N'M'} = \int_0^\infty d\omega \frac{J_{NM,N'M'}(\omega)}{\omega}. \tag{13}$$

Reorganization energy is related to the system-bath coupling strength, and the lineshape function describes how correlations between different site energy or couplings affect relaxation dynamics. To describe the continuous nature of the bath mode distribution, we have used a generalized spectral density

$$J_{NM,N'M'}(\omega) = \sum_i g_{NM,i}\, g_{N'M',i}\Lambda_{NM,N'M',i}\, \omega_i\, \delta(\omega_i - \omega), \tag{14}$$

where $\Lambda_{NM,N'M'„i}$ is a scaling parameter. A generalized spectral density can delineate correlations between site energy fluctuation, coupling fluctuation, and cross-correlations between them. For example, when $N = M$ and $N' = M'$, it reduces to $J_{NN,N'N'}(\omega)$. It is a spectral density of site energy fluctuation on the Nth vibronic state, $J_{NN}(\omega)$, when $N = N'$ and it is a spectral density of a cross-correlation between energy fluctuation on the Nth and Mth vibronic state, $J_{NM}(\omega)$, when $N \neq M$. Particularly, $J_{NM,MN}(\omega)$, a spectral density of coupling fluctuation between the Nth vibronic state and Mth vibronic state leads to vibrational relaxation in our extended modified Redfield theory if they refer to different vibrational states on the same monomer (e.g., $|N\rangle = |n, n_v\rangle$ and $|M\rangle = |n, n_v'\rangle$ where $n_v \neq n_v'$). To see why off-diagonal elements of system bath couplings lead to coupling fluctuation clearly, we express the lineshape function $g_{NM,MN}(t)$, a function of $J_{NM,MN}(\omega)$ from Eq. 12, in an alternative form

$$g_{NM,MN}(t) = \frac{1}{\hbar^2}\int_0^t d\tau \int_0^\tau d\tau' \left\langle H_{sb}^{NM}(\tau)H_{sb}^{MN}(\tau')\right\rangle_B = \frac{1}{\hbar^2}\int_0^t d\tau \int_0^\tau d\tau' \left\langle H_{sb}^{NM}(\tau)H^{\dagger}{}_{sb}^{NM}(\tau')\right\rangle_B, \tag{15}$$

here $\left\langle H_{sb}^{NM}(\tau)H^{\dagger}{}_{sb}^{NM}(\tau')\right\rangle_B$ is an autocorrelation function of fluctuation coupling between the Nth vibronic state and Mth vibronic state.

Though $J_{NM,N'M'}(\omega)$ is capable of describing all kinds of system-bath interactions, we did not include all of them in our simulation. We make only

$$J_{NN,NN}(\omega) = \sum_i g_{NN,i}^2\, \omega_i^2 \delta(\omega_i - \omega), \tag{16}$$

$$J_{NM,MN}(\omega) = \sum_i g_{NM,i} g_{MN,i} \Lambda_{NM,MN,i} \omega_i^2 \delta(\omega_i - \omega) \tag{17}$$

$$J_{NN,MM}(\omega) = \sum_i g_{NN,i} g_{MM,i} \Lambda_{NN,MM,i} \omega_i^2 \delta(\omega_i - \omega), \tag{18}$$

nonzero and set their scaling parameters to be unity. $J_{NN,NN}(\omega)$ is the spectral density of site energy fluctuation, and we applied it to all states. $J_{NM,MN}(\omega)$ is the spectral density of coupling fluctuation, and to focus on the effect of vibrational relaxation toward the energy transfer dynamics in a vibronic system, we only consider the coupling fluctuation between different vibrational states on the same monomer (e.g., $n = m$ but $n_v \neq m_v$), and ignore the coupling fluctuation between states on different monomers (e.g., $n \neq m$), i.e., the excitonic coupling fluctuation. $J_{NN,MM}(\omega)$ is the spectral density of the correlation between energy fluctuation of two different vibronic states, and we used it to make different vibrational states on the same monomer become correlated states ($\Lambda_{NN,MM,i} = 1$) since energy gap fluctuation of an electronic state is usually larger than energy gap fluctuation of a vibrational state. Consequently, vibrational states experience identical bath motions, and they have a fixed energy gap. With these spectral densities, $J_{NM,MN}(\omega)$ induces coupling fluctuation to allow transitions between vibrational states, even when $\left\langle V_{n,n_v;m=n,m_v\neq n_v}\right\rangle = 0$, and this is the vibrational relaxation. A graphical demonstration of our idea is shown in Figure 2. The inclusion of the other terms from the above generalized spectral density, e.g., correlation between energy fluctuation and coupling fluctuation $J_{NN,NM}(\omega)$, could also impact excitation energy transfer dynamics[28, 29], but inclusion of these more sophisticated system-bath interactions requires more experimental or simulated inputs to justify their usages and such discussion is beyond the scope of this work.

In our simulation, different spectral densities were used for energy gap fluctuation and coupling fluctuation between vibrational states on the same monomer. For brevity, we will use $J_{ele}(\omega)$ and $J_{vib}(\omega)$ to denote these two spectral densities, respectively. To accurately capture the protein-chromophore interaction of dimers in APC, we adopted a detailed-structural spectral density for site energy gap fluctuation. It has a general form of

$$J_{MBO}(\omega) = \sum_k \frac{p_k \omega}{[(\omega - \Omega_k)^2 + \Gamma_k^2][(\omega + \Omega_k)^2 + \Gamma_k^2]}, \tag{19}$$

which was originally proposed by Meier and Tanner[30, 31], and it is hereafter called the multimode Brownian oscillator (MBO) spectral density hereinafter. p_k, Ω_k and Γ_k are arbitrary parameters, and they are determined by fitting the vibrational coherence signals from the broad-band pump-probe experiment of intact phycobilisomes. Details of the broad-band pump-probe experiment and the following processing and fitting have been reported in previous work (cite CPC manuscript). To obtain the spectral density that best represents the protein environment of dimers in APC, the vibrational coherence signals at the emission wavelength of 655 nm is selected, which is the absorption maximum of APC. The resultant spectral density is plotted in **Figure 1c**. In addition, since the HOOP mode is already in the system Hamiltonian, it was removed from the $J_{MBO}(\omega)$ to avoid double counting. We note that when we refer to the total reorganization energy of the MBO spectral density λ_{MBO}, it will still contain the reorganization energy of the HOOP mode for clarity although it is not really included in the system-bath Hamiltonian. Additionally, to compensate

for the extreme low-frequency mode that could not be observed in the broad-band pump-probe experiment, we employed an overdamped (OD) spectral density

$$J_{OD}(\omega) = \frac{2\lambda_{OD}}{\pi}\frac{\omega\Lambda}{\omega^2 + \Lambda^2}. \quad (20)$$

We set the λ_{OD} to be 10 cm^{-1} and Λ to be 283 fs^{-1}[15]. The inclusion of OD spectral density is again to help us achieve a more realistic protein environment in APC, and it does not significantly alter our conclusion. The resultant spectral density of site energy fluctuation is

$$J_{ele}(\omega) = J_{MBO}(\omega) + J_{OD}(\omega) \quad (21)$$

On the other hand, we utilized an Ohmic spectral density for the spectral density of coupling fluctuation

$$J_{vib}(\omega) = \lambda_{vib}\frac{\omega}{\omega_c}e^{-\frac{\omega}{\omega_c}}, \quad (22)$$

where ω_c is a cut-off frequency, and λ_{vib} is the reorganization energy of a coupling element. When the bath of electronic degrees of freedom is described by the multimode Brownian oscillator, the thermal bath of a vibrational mode can be delineated by an Ohmic spectral density, as shown by Bennett et al.[20] and Garg et al.[32] The vibrational relaxation time constant is reported to be 120 fs from a hole-burning detection pump-probe by Beck and coworkers[11]. Therefore, parameters of $J_{vib}(\omega)$ are determined by simulating a pure vibrational relaxation process to yield this 120-fs experimental relaxation time constant. The details of parameters determination are in supporting information. Throughout this study, we assume an identical and independent bath for all states except for those vibrational states on the same monomer which have a correlated bath.

Model parameters

Here, we describe the system parameters used in the simulations. The dipole-dipole coupling between two monomers, $V_{\alpha\beta}$, is -160 cm^{-1} in our simulations as reported by Beck and coworkers[9]. The site energy difference of the α_{84}-β_{84} chromophore dimer in APC has been reported to range from 750 to 800 cm^{-1} by multiple studies[9, 33]. To understand the role of the HOOP mode in enhancing energy transfer, we calculated the excitation energy transfer rate across a wide range of site energies. We also varied the reorganization energy of $J_{MBO}(\omega)$ to observe the impact of bath coupling on EET dynamics. The Franck-Condon factor of the HOOP modes is calculated using the Huang-Rhys factor, defined as:

$$s = s_{HOOP} = \frac{\lambda_{HOOP}}{\hbar\omega_{HOOP}}. \quad (23)$$

Subsequently, the corresponding Franck-Condon factor is determined as:

$$S_{\alpha,0n_v} = \sqrt{e^{-s}\frac{s^{n_v}}{n_v!}}. \quad (24)$$

Given that the frequency of the HOOP mode (818 cm^{-1}) is more than four times the room temperature thermal energy (200 cm^{-1}), considering up to $n_v = 1$ vibrational states will be adequate to capture realistic

dynamics. The Franck-Condon factors are normalized to satisfy $\sum_{n_v} S_{0n_v}^2 = 1$. Additionally, while varying the reorganization energy of $J_{MBO}(\omega)$, the Huang-Rhys changes. The λ_{HOOP} is given by $\lambda_{MBO}\eta$, where η represents the ratio of the HOOP mode reorganization energy to the total reorganization energy of MBO spectral density, and η is set at 0.050 in this study.

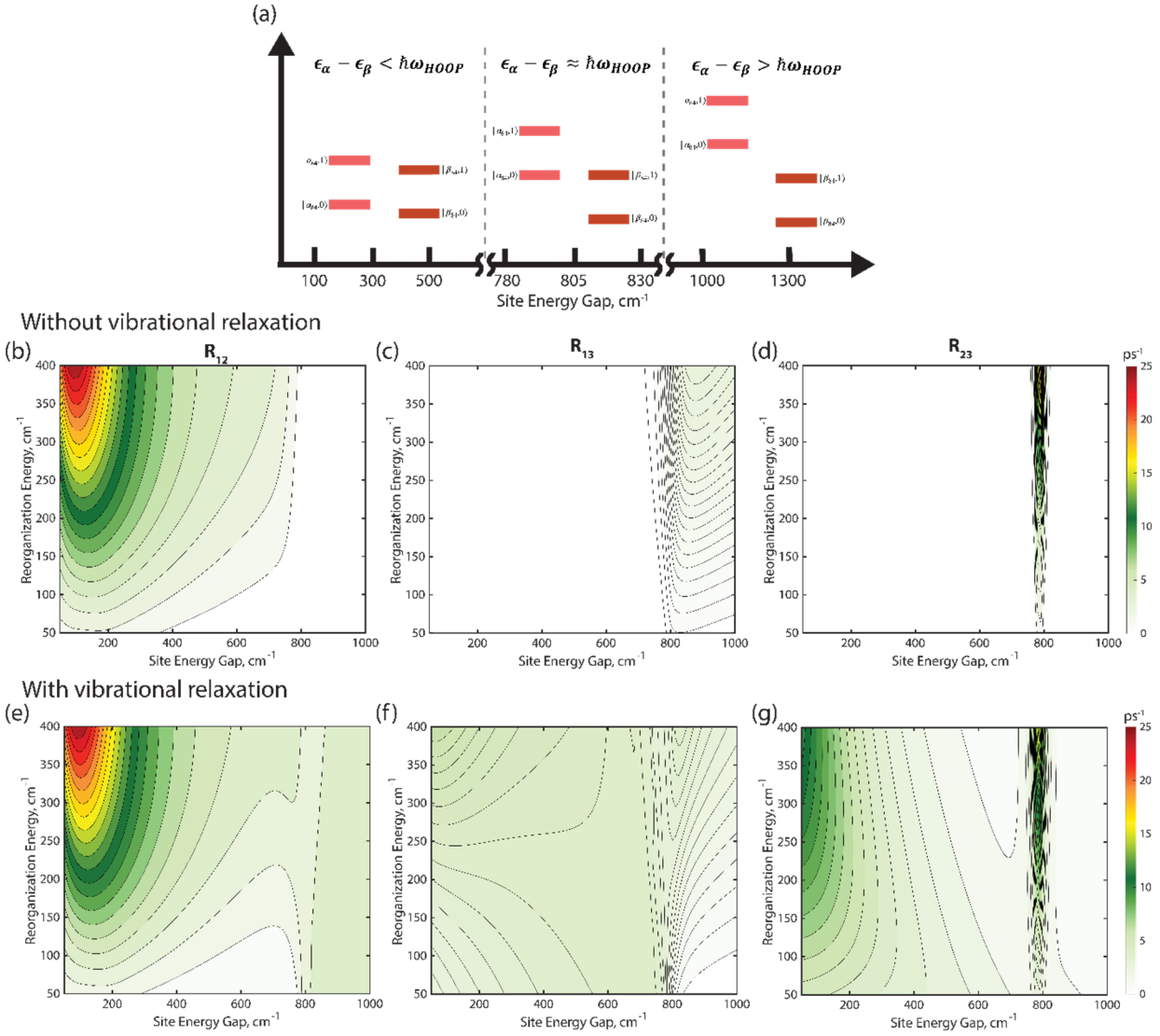

Figure 3: States of the α_{84}-β_{84} chromophore dimer in the site basis with different site energies and 2D maps of modified Redfield rates as a function of the site energy gap and reorganization energy of the MBO spectral density. (a) Site basis states of chromophore dimer under the small energy gap ($\epsilon_\alpha - \epsilon_\beta < \hbar\omega_{HOOP}$), near resonant ($\epsilon_\alpha - \epsilon_\beta \approx \hbar\omega_{HOOP}$) and the large energy gap condition ($\epsilon_\alpha - \epsilon_\beta > \hbar\omega_{HOOP}$). (b)-(d) Plots of downhill modified Redfield rates of $|e_2\rangle$ to $|e_1\rangle$, $|e_3\rangle$ to $|e_1\rangle$ and $|e_3\rangle$ to $|e_2\rangle$ transitions under different site energy gaps and reorganization energy of energy gap fluctuation without vibrational relaxation. (e)-(g) Plots of modified Redfield rates of $|e_2\rangle$ to $|e_1\rangle$, $|e_3\rangle$ to $|e_1\rangle$ and $|e_3\rangle$ to $|e_2\rangle$ transitions including vibrational relaxation. All plots share the same color bar scheme.

Dynamics from Modified Redfield rate calculations without vibrational relaxation

To understand the role of vibrational relaxation in speeding up the excitation energy transfer in the α_{84}-β_{84} chromophore dimer, we first calculated the energy transfer rates between different eigenstates without incorporating vibrational relaxation. **Figure 3b-d** show 2D maps of the calculated rates as a function of site energy gap and reorganization energy in the absence of vibrational relaxation. The results are consistent with Moran and Womick's[15] results, despite using different Huang-Rhys factors and utilizing detailed-structure protein bath modes. To aid interpretation, the site basis energy states are depicted in Figure 3a, corresponding to the small site energy gap ($\epsilon_\alpha - \epsilon_\beta < \hbar\omega_{HOOP}$), the near resonant energy gap ($\epsilon_\alpha - \epsilon_\beta \approx \hbar\omega_{HOOP}$) and the large site energy gap ($\epsilon_\alpha - \epsilon_\beta > \hbar\omega_{HOOP}$) conditions from left to right. When the site energy gap is small, the lowest two eigenstates, $|e_1\rangle$ and $|e_2\rangle$, mainly comprise states $|\beta_{84}, 0\rangle$ and $|\alpha_{84}, 0\rangle$. We only observed a pronounced energy transfer rate from$|e_2\rangle$ to $|e_1\rangle$, i.e., R_{12} in Figure 3b. This observation is explained by the low Huang-Rhys factor of the HOOP mode which makes only $|\beta_{84}, 0\rangle$ and $|\alpha_{84}, 0\rangle$ appreciably coupled. In the large site energy gap condition, we found significant energy transfer from $|e_3\rangle$ to $|e_1\rangle$, i.e., R_{13} in **Figure 3c**. It is worth noting that $|e_3\rangle$ has most $|\alpha_{84}, 0\rangle$ state feature in this condition. This observation implies the same physical picture as in the small energy gap condition, where the energy transfer from $|\alpha_{84}, 0\rangle$ to $|\beta_{84}, 0\rangle$ dominates. Although $|\alpha_{84}, 0\rangle$ and $|\beta_{84}, 1\rangle$ are close in energy, no noticeable R_{23} appears in **Figure 3d** because of the drastically low coupling between these two states in comparison to the coupling between $|\alpha_{84}, 0\rangle$ and $|\beta_{84}, 0\rangle$. For example, $V_{\alpha_{84},0;\beta_{84},0} = V_{\alpha_{84}\beta_{84}} S_{\alpha_{84},00} S_{\beta_{84},00}$ is -157.1 cm^{-1} and $V_{\beta_{84},1;\alpha_{84},0}$ is -21 cm^{-1} given s_{HOOP} is 0.018 while λ_{MBO} is 300 cm^{-1}.

In the near-resonant condition, the site energy gap is close to the frequency of the HOOP mode, therefore $|\alpha_{84}, 0\rangle$ and $|\beta_{84}, 1\rangle$ states are strongly mixed and form excitonic eigenstates $|e_2\rangle$ and $|e_3\rangle$. In **Figure 3d**, an intense and narrow resonant peak emerges at the site energy gap of 790 cm^{-1}, representing a rapid energy transfer driven by the resonance between the $|\alpha_{84}, 0\rangle$ and $|\beta_{84}, 1\rangle$ states. Additionally, the 790 cm^{-1} site energy gap correlates well with the reported site energy gap of the α_{84}-β_{84} chromophore dimer in APC[7], indicating the significant role of the HOOP mode in the energy transfer of the dimer system. We notice that this resonant peak does not appear at the exact frequency of the HOOP mode, 818 cm^{-1}, mainly due to the non-zero couplings between $|\alpha_{84}, 1\rangle$ and $|\beta_{84}, 1\rangle$ and between $|\alpha_{84}, 0\rangle$ and $|\beta_{84}, 0\rangle$. The presence of these couplings pushes $|e_2\rangle$ and $|e_3\rangle$ away from each other in energy when $\epsilon_\alpha - \epsilon_\beta = \hbar\omega_{HOOP}$, and therefore, the actual resonant condition, i.e., the site energy gap leading to the lowest excitonic energy gap between $|e_2\rangle$ and $|e_3\rangle$, occurs when the site energy gap has a slightly lower value than the frequency of HOOP mode in a vibronic exciton model.

These simulation results hint that the HOOP mode resonantly enhances the energy transfer rate between α_{84}-β_{84} chromophore dimers. However, this model does not explain rapid energy capture by the $|\beta_{84}, 0\rangle$ state. In other words, the model does not successfully describe the overall downhill energy transfer process recently observed by Schlau-Cohen and coworkers with narrowband single-molecule pump-probe spectroscopy[16]. While rapid energy transfer from $|e_3\rangle$ to $|e_2\rangle$ is observed, the results predict no rapid relaxation into lowest energy state, i.e., $|e_1\rangle$. The calculation based on the site energy gap of 790 cm^{-1} and the reorganization energy of 300 cm^{-1} yields $R_{23} = 10.45$ ps^{-1} (τ_{23}= 96 fs), $R_{13} = 0.742$ ps^{-1} (τ_{13} = 1347 fs) and $R_{12} = 0.682$ ps^{-1} (τ_{12} = 1466 fs). Despite the large R_{23}, low R_{13} and R_{12} impede relaxation into $|e_1\rangle$. While obtaining the rate in site basis is not feasible due to the absence of coherence elements in modified Redfield theory, we could still investigate these rates by a simple analysis: when $|e_2\rangle$ and $|e_3\rangle$ have the minimal excitonic energy gap, the composition ratio of $|\alpha_{84}, 0\rangle$ and $|\beta_{84}, 1\rangle$ in these two eigenstates will be equal, with different or the same sign depending on the antibonding or bonding like features of eigenstates. Consequently, a rapid population transfer from $|e_3\rangle$ to $|e_2\rangle$ does not necessarily imply the rapid site population transfer from the chromophore around α_{84} to the one around β_{84}. Furthermore, considering that the transition dipole moment between the ground electronic state and $|\alpha_{84}, 0\rangle$ is much larger than the transition dipole moment between the ground electronic state and $|\beta_{84}, 1\rangle$, due to the small Huang-Rhys factor of the HOOP mode, the photoexcitation in an ultrafast spectroscopic experiment will lead to the nearly same initial population in $|e_2\rangle$ and $|e_3\rangle$. When combined with the fact

that the reverse population transfer from state $|e_2\rangle$ to $|e_3\rangle$ is also fast given the small energy gap between two near resonant states, no significant net population transfer occurs even with a large R_{23}.

To summarize, incorporating the HOOP mode into a vibronic exciton model successfully demonstrates the rapid energy transfer rate from $|e_3\rangle$ to $|e_2\rangle$, as also shown by Womick and Moran[15]. Recently, Schlau-Cohen and coworkers[16] demonstrated however, that transfer of the exciton explicitly to spectrally redshifted $|e_1\rangle$ state is also rapid. These signatures were observed in the experiments of Beck and coworkers. Schlau-Cohen and coworkers also demonstrated that transfer and relaxation operate simultaneously to enable rapid energy capture by the lowest energy state. To incorporate this aspect of the dynamics into the model, vibrational relaxation will have to be included in the dynamics. In this model, vibrational relaxation can be added to occur from $|\beta_{84}, 1\rangle$ to $|\beta_{84}, 0\rangle$, a process essential for the rapid relaxation from $|e_2\rangle$ to $|e_1\rangle$. Given that $|e_1\rangle$ is a localized state of the chromophore around β_{84} under the near-resonant condition, incorporating such vibrational relaxation into the modified Redfield rate calculations would offer a more comprehensive physical depiction and provide better insights into recent experimental outcomes.

Dynamics after incorporating vibrational relaxation into modified Redfield rate

We next calculated the energy transfer rates after incorporating vibrational relaxation into modified Redfield theory as described previously. The spectral density parameters to calculate dynamic fluctuation in coupling are $\lambda_{vib} = 300\ cm^{-1}$ and $\omega_c = 200\ cm^{-1}$. In practice, since there is no simple analytical solution for the lineshape function of an Ohmic spectral density, we once again utilized the multimode Brownian oscillator spectral density proposed by Meier and Tannor[30, 31]to numerically calculate the lineshape function of coupling fluctuation. For these coupling fluctuation parameters, a single Brownian oscillator spectral density with p = 4.31×10^{10}(cm^{-1})^4, $\Omega = 100$ cm^{-1} and $\Gamma = 320$ cm^{-1} was used. These parameters resulted in a vibrational relaxation time constant of 117 fs, which aligns well with the relaxation time obtained from the hole-burning detection pump-probe experiment[11] (120 fs). Details of parameters determination are presented in supporting information. The calculated rates are plotted in **Figure 3e-g**. We observe that **Figure 3e-g** are not distinct from **Figure 3b-d**, where the transitions are solely due to Coulombic interactions, as well as new features arising from transitions caused by vibrational relaxation. To systematically analyze the vibrational relaxation induced transition, we once again categorized the electronic structure into three different scenarios. We will discuss each case in detail.

When the site energy gap is small, vibrational relaxation results in new pronounced transitions from $|e_3\rangle$ to $|e_2\rangle$ and from $|e_3\rangle$ to $|e_1\rangle$, as depicted in **Figure 3f** and **Figure 3g**. The impact of reorganization energy on energy transfer rates is non-monotonic. The rates increase with larger reorganization energy in the regime of small site energy gaps but begins to decrease as the energy gap approaches around 400 cm^{-1}. It is important to note reorganization energy mentioned here pertains to site energy fluctuation, as the reorganization energy of coupling fluctuation remains constant. This trend could be explained by considering that when the site energy is small, the energy difference between $|e_3\rangle$ and $|e_2\rangle$ is large, making it difficult for these states to access bath modes that provide strong coupling fluctuation. However, energy gap fluctuation can bridge this large energy difference, causing R_{23} to increase with larger reorganization energy. On the other hand, as the site energy gap becomes larger, the energy difference between $|e_3\rangle$ and $|e_2\rangle$ decreases and energy gap fluctuation hinders the access of $|e_3\rangle$ and $|e_2\rangle$ to bath modes offering strong coupling fluctuation. Additionally, in the large energy gap condition, a new transition occurs in R_{12}, and the rate is independent of the reorganization energy. This is due to the fact that $|e_2\rangle$ has high percentage of $|\beta_{84}, 1\rangle$ character (e.g., 96.7% at the site energy gap of 900 cm^{-1}), which results in $|e_2\rangle$ access to the vibrational relaxation pathway from $|\beta_{84}, 1\rangle$ to $|\beta_{84}, 0\rangle$ in the site basis. R_{13} in large energy gap regime also changes because $|e_3\rangle$ has a small amount of the $|\beta_{84}, 1\rangle$ component (e.g., 3.3% at the site energy gap of 900 cm^{-1}), leading to a combined effect of the Coulombic interaction and vibrational relaxation, where the Coulombic interaction remains dominant.

Lastly, we examine EET at the resonant condition. Once again, we find an enhanced, rapid energy transfer rate in R_{23} at the site energy gap of 790 cm^{-1}. This enhanced peak does not differ from the peak in

Figure 3d since the Coulombic interaction remains dominant in the energy transfer process. Nonetheless we now clearly observe appreciably faster R_{12} and R_{13} energy transfer rates due to the incorporation of vibrational relaxation into the modified Redfield calculation. For example, at the point $(\Delta E, \lambda_{ele})$ = (790, 300) cm^{-1}, τ_{12} is 357 fs and τ_{13} is 386 fs; these values are 3-4 times shorter than time constants obtained without the inclusion of vibrational relaxation. The fast energy transfer rates from $|e_3\rangle$ into $|e_1\rangle$ and $|e_2\rangle$ into $|e_1\rangle$ imply rapid energy localization on $|\beta, 0\rangle$ state, which completes the energy transfer process from the α_{84} chromophore to the β_{84} chromophore in allophycocyanin. This result clearly demonstrates the essential role of vibrational relaxation to describe a complete energy transfer process in a vibronic exciton model. Without the vibrational relaxation, we can only see the rapid energy transfer between $|e_3\rangle$ and $|e_2\rangle$ as shown in Figure 3d, but no pronounced energy capture by the lowest energy excitonic state occurs. While vibrational enhancement of the excitation energy transfer rate is common in the photosynthetic systems or light-harvesting antenna[2], the inclusion of vibrational relaxation into a simulation is essential for a holistic view of energy transfer dynamics.

So far, our calculation is performed using the MRT with inclusion of vibrational relaxation. However, as mentioned above, MRT ignores the coherence elements of a density matrix, so it is impossible to obtain the site basis information. Still, looking into the dynamics in site basis is desirable since it makes the energy transfer more intuitive. Therefore, to go beyond this limit, and to have a more in-depth analysis, we performed a quantum dynamics simulation of the system with ΔE_{site} of 790 cm^{-1} and λ_{ele} of 300 cm^{-1} using coherent modified Redfield theory (CMRT) developed by the Cheng group[34, 35]. CMRT is an extension of modified Redfield theory which includes the time evolution of coherence, enabling direct examination of site basis population transfer through the unitary transformation. While there are other means to delineate the EET dynamics including coherence evolution, such as the polaron transformation approaches (e.g., Coherent resonant energy transfer[36]), our idea of incorporating the vibrational relaxation effect by introducing coupling fluctuation can be seamlessly integrated into CMRT. The resultant rate equations once again retain their original forms (derivation is shown in supporting information). Therefore, we can now compare the dynamics propagated by CMRT with and without the vibrational relaxation to further reveal the necessity for incorporating vibrational relaxation in modeling excitation energy transfer of α_{84}-β_{84} chromophore dimers in APC.

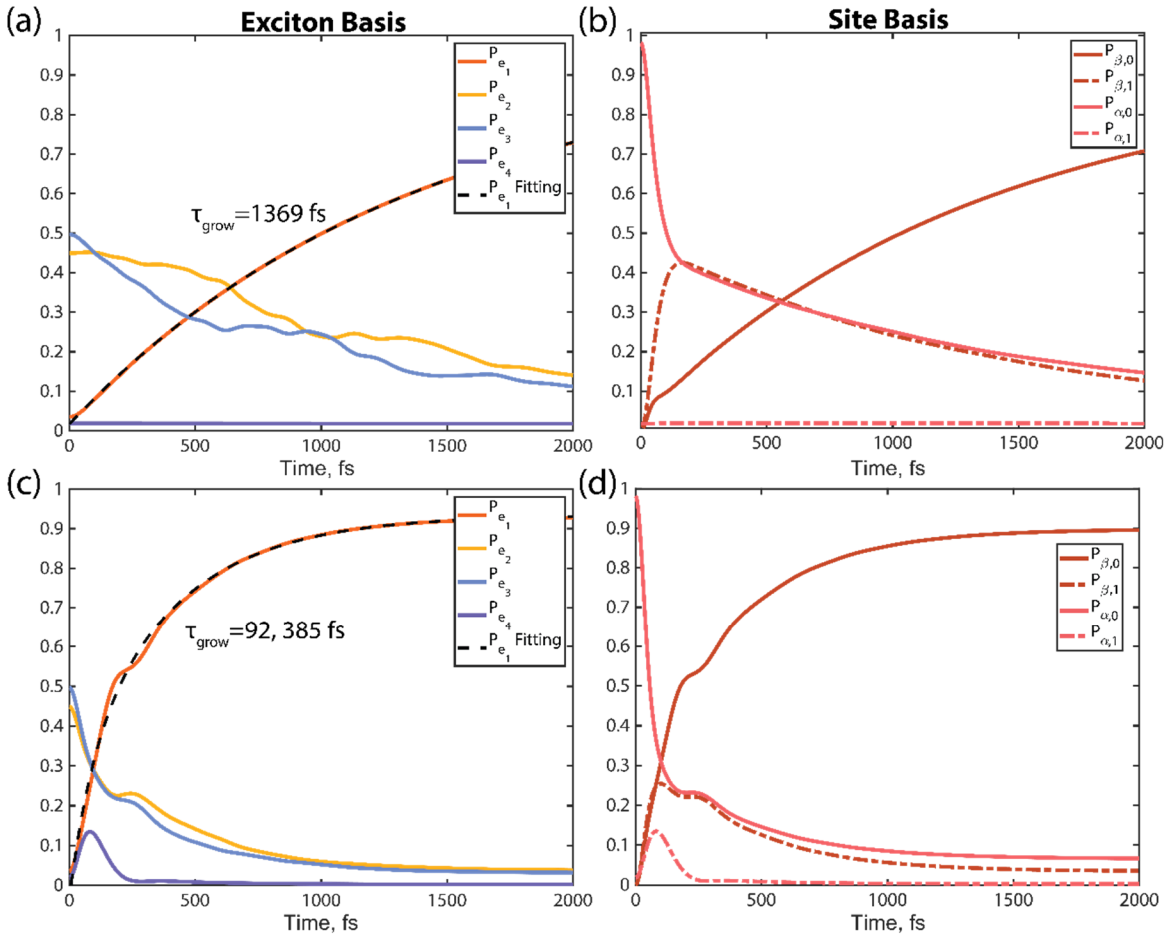

Figure 4: Population dynamics given by coherent modified Redfield theory (CMRT) with and without the inclusion of vibrational relaxation. The initial condition was set at complete occupation of the α_{84} site, and the simulation time goes from 0 to 2000 fs with 1 fs time step. (a) and (b) are the population dynamics in exciton basis and site basis, respectively, without the vibrational relaxation. We fit the growth of $|e_1\rangle$ population with a function $P_{e_1}(t) = A - Be^{-t/\tau_{grow}}$ to extract the population growth and it yields a rise time of 1369 fs. (c) and (d) are the population dynamics in exciton basis and site basis respectively with the vibrational relaxation. A fitting with function $P_{e_1}(t) = A - Be^{-t/\tau_{grow,1}} - Ce^{-t/\tau_{grow,2}}$ yields the rise time of 92 and 385 fs.

To explore the role of the vibrational relaxation process, an artificial initial condition was used where only the α_{84} site is initially populated. The simulation results are plotted in **Figure 4**. The top two figures illustrate the population dynamics in excitonic and site bases without vibrational relaxation. Although the population transfer from $|\alpha, 0\rangle$ to $|\beta, 1\rangle$ occurs within the first 100 fs, the energy transfer towards $|\beta, 0\rangle$ proceeds slowly with a time constant of 1369 fs. This is attributed to the absence of any transfer mechanisms apart from the Coulomb interaction between $|\beta, 0\rangle$ and $|\alpha, 0\rangle$. Upon considering vibrational relaxation, we observe both the rapid population transfer from $|\alpha, 0\rangle$ to $|\beta, 1\rangle$ and the swift relaxation towards $|\beta, 0\rangle$ as shown in **Figure 4d**. A biexponential fitting of the dynamics of $P_{\beta,0}$ in Figure 4d yields the time constants of $\tau = 92$ and 385 fs, and a single exponential fitting (**Figure S2**) gives $\tau =$ 303 fs, which aligns well with the time constants obtained from the anisotropic experiment[7] (280 fs), photo-echo experiment[10] (220 fs), and the recent single-molecule pump-probe experiments by Schlau-Cohen and coworkers[16] (140 fs). Additionally, in attempt to give an insight into the bifurcation of energy transfer time constants in APC observed in the single-molecule pump-probe experiment, we perform a simulation

combining the utilization of a broad and biased site energy gap distribution to mimic the large heterogeneity of the APC protein environment and our model. Our results indicate the bifurcation of energy transfer time constants may stem from the tuning or detuning of the site energy gap between two monomers from resonating with the HOOP mode by the large heterogeneity of protein. More details and discussion of the simulation are in supporting information. With this more direct observation of energy transfer in both site and eigenbasis and the capability of looking into the origin of time constant bifurcation in the single-molecule pump-probe experiment, we again show that vibrational relaxation in a vibronic exciton model is imperative for a comprehensive understanding of the excitation energy transfer in allophycocyanin.

In this work, we incorporate vibrational relaxation in a vibronic exciton model into modified Redfield theory to describe the energy transfer process between strongly coupled α_{84} and β_{84} chromophore dimers in allophycocyanin. Our approach accurately models a rapid population transfer within two near-degenerate vibronic states and the relaxation into the localized low-energy state. Our results show that the 818 cm^{-1} hydrogen-out-of-plane mode not only resonantly enhances the transition between nearly resonant states $|\alpha, 0\rangle$ and $|\beta, 1\rangle$, but also offers an excitation on the $|\alpha, 0\rangle$ state rapid access to the vibrational relaxation mechanism of the β_{84} chromophore. Access to this vibrational relaxation pathway in our model makes the energy capture rate fast and efficient, as is observed experimentally (280 fs). In particular, our formalism represents transport in both space and energy; that is, energy moves from the α_{84} chromophore to β_{84} not merely as a consequence of coherent oscillation but the excitation actually localizes to the lower energy $|\beta_{84}, 0\rangle$ state giving a better correspondence with previous energy transfer rates observed in ultrafast spectroscopy and microscopy experiments. In our model, dynamics is initiated by vibronic coherence which provides rapid motions or the delocalization between near-resonant coupled states. At the same time, the actual relaxation, capture, and localization occur due to vibrational relaxation on the acceptor chromophore.

MRT with vibrational relaxation could be easily applied to systems with vibrational-assisted energy transfer processes. For instance, Policht et. al.[17] recently discovered the vibronic structure in the bacterial reaction center and observed a vibronically coherent transfer in two-dimensional electronic spectroscopy experiments. Similarly, investigations on LHCII[37] also revealed vibration-assisted energy transfer. Our method also has the potential to be applied to other light-harvesting complexes[2], conjugated donor-acceptor materials[38, 39] and polaritonic systems[40]. As the interplay between electronic states and vibrational modes continues to be revealed by ultrafast spectroscopic studies, new approaches to modeling energy transfer and capture mechanisms will be required. We herein demonstrate the importance of introducing vibrational relaxation in a vibronic exciton model and how it accurately captures the excitation energy transfer process as well as the energy localization.

While in this study we only include vibrational relaxation in MRT and its extension, CMRT, our approach also shows the generality and feasibility of introducing vibrational relaxation into vibronic exciton dynamics in other existing theoretical frameworks. For example, it is possible, though challenging, to integrate coupling fluctuation into quantum dynamics simulation methods using polaron-transformation, e.g., coherent resonant energy transfer (CRET) method and its derivatives. These extensions could describe vibrational relaxation and dynamic localization in an EET process simultaneously, where the dynamical localization has been shown to be a significant process in EET of photosynthetic systems[41].

Supporting Information

1 file: Method derivation, details of parameters determination, simulation details, comparison to other experiments.

Acknowledgments

We thank Professor Tomáš Mančal for a discussion on Modified Redfield theory. We thank Professor C. Neil Hunter, Dr. Craig MacGregor-Chatwin and Dr. Andrew Hitchcock for providing us with phycobilisome samples. We thank Dr. Karen M. Watters for scientific editing. P.-J.W. acknowledges the Department of Chemistry at the University of Chicago for the Eugene Olshansky Memorial Fellowship for funding. S.S.

thanks Department of Chemistry, University of Chicago for the Benjamin Ball Freud Merit Scholarship for funding. This work was primarily funded by the Department of Energy through Award No. DE-SC0020131 and also benefitted from the financial support provided by the National Science Foundation through QuBBE QLCI (NSF OMA-2121044) and Grant No. CHE-1900359.

References

(1) Domínguez-Martín, M. A.; Sauer, P. V.; Kirst, H.; Sutter, M.; Bína, D.; Greber, B. J.; Nogales, E.; Polívka, T.; Kerfeld, C. A. Structures of a phycobilisome in light-harvesting and photoprotected states. *Nature* **2022**, *609* (7928), 835-845. DOI: 10.1038/s41586-022-05156-4.
(2) Mirkovic, T.; Ostroumov, E. E.; Anna, J. M.; Grondelle, R. v.; Govindjee; Scholes, G. D. Light Absorption and Energy Transfer in the Antenna Complexes of Photosynthetic Organisms. *Chem. Rev.* **2017**, *117* (2), 249-293. DOI: 10.1021/acs.chemrev.6b00002.
(3) Cheng, Y.-C.; Fleming, G. R. Dynamics of Light Harvesting in Photosynthesis. *Annu. Rev. Phys. Chem.* **2009**, *60* (Volume 60, 2009), 241-262. DOI: 10.1146/annurev.physchem.040808.090259.
(4) Kolodny, Y.; Avrahami, Y.; Zer, H.; Frada, M. J.; Paltiel, Y.; Keren, N. Phycobilisome light-harvesting efficiency in natural populations of the marine cyanobacteria Synechococcus increases with depth. *Commun. Biol.* **2022**, *5* (1), 727. DOI: 10.1038/s42003-022-03677-2.
(5) Liu, H.; Zhang, H.; Niedzwiedzki, D. M.; Prado, M.; He, G.; Gross, M. L.; Blankenship, R. E. Phycobilisomes Supply Excitations to Both Photosystems in a Megacomplex in Cyanobacteria. *Science* **2013**, *342* (6162), 1104-1107. DOI: 10.1126/science.1242321.
(6) Womick, J. M.; Moran, A. M. Nature of Excited States and Relaxation Mechanisms in C-Phycocyanin. *J. Phys. Chem. B* **2009**, *113* (48), 15771-15782. DOI: 10.1021/jp908093x.
(7) Womick, J. M.; Moran, A. M. Exciton Coherence and Energy Transport in the Light-Harvesting Dimers of Allophycocyanin. *J. Phys. Chem. B* **2009**, *113* (48), 15747-15759. DOI: 10.1021/jp907644h.
(8) Sohoni, S.; Lloyd, L. T.; Hitchcock, A.; MacGregor-Chatwin, C.; Iwanicki, A.; Ghosh, I.; Shen, Q.; Hunter, C. N.; Engel, G. S. Phycobilisome's Exciton Transfer Efficiency Relies on an Energetic Funnel Driven by Chromophore–Linker Protein Interactions. *J. Am. Chem. Soc.* **2023**, *145* (21), 11659-11668. DOI: 10.1021/jacs.3c01799.
(9) Sil, S.; Tilluck, R. W.; M, N. M. T.; Leslie, C. H.; Rose, J. B.; Domínguez-Martín, M. A.; Lou, W.; Kerfeld, C. A.; Beck, W. F. Excitation energy transfer and vibronic coherence in intact phycobilisomes. *Nat. Chem.* **2022**, *14* (11), 1286-1294. DOI: 10.1038/s41557-022-01026-8.
(10) Homoelle, B. J.; Edington, M. D.; Diffey, W. M.; Beck, W. F. Stimulated Photon-Echo and Transient-Grating Studies of Protein-Matrix Solvation Dynamics and Interexciton-State Radiationless Decay in α Phycocyanin and Allophycocyanin. *J. Phys. Chem. B* **1998**, *102* (16), 3044-3052. DOI: 10.1021/jp972782x.
(11) Edington, M. D.; Riter, R. E.; Beck, W. F. Femtosecond Transient Hole-Burning Detection of Interexciton-State Radiationless Decay in Allophycocyanin Trimers. *J. Phys. Chem. B* **1997**, *101* (22), 4473-4477. DOI: 10.1021/jp970424o.
(12) Gillbro, T.; Sharkov, A. V.; Kryukov, I. V.; Khoroshilov, E. V.; Kryukov, P. G.; Fischer, R.; Scheer, H. Förster energy transfer between neighbouring chromophores in C-phycocyanin trimers. *Biochim. Biophys. Acta (BBA) - Bioenerg.* **1993**, *1140* (3), 321-326. DOI: 10.1016/0005-2728(93)90072-n.

(13) Sauer, K.; Scheer, H. Excitation transfer in C-phycocyanin. Förster transfer rate and exciton calculations based on new crystal structure data for C-phycocyanins from Agmenellum quadruplicatum and Mastigocladus laminosus. *Biochim. Biophys. Acta (BBA) - Bioenerg.* **1988**, *936* (2), 157-170. DOI: 10.1016/0005-2728(88)90232-0.
(14) Sui; Sen, F. Structure of Phycobilisomes. *Annual Review of Biophysics* **2021**, *50* (Volume 50, 2021), 53-72. DOI: 10.1146/annurev-biophys-062920-063657.
(15) Womick, J. M.; Moran, A. M. Vibronic Enhancement of Exciton Sizes and Energy Transport in Photosynthetic Complexes. *J. Phys. Chem. B* **2011**, *115* (6), 1347-1356. DOI: 10.1021/jp106713q.
(16) Moya, R.; Norris, A. C.; Kondo, T.; Schlau-Cohen, G. S. Observation of robust energy transfer in the photosynthetic protein allophycocyanin using single-molecule pump–probe spectroscopy. *Nat. Chem.* **2022**, *14* (2), 153-159. DOI: 10.1038/s41557-021-00841-9.
(17) Policht, V. R.; Niedringhaus, A.; Willow, R.; Laible, P. D.; Bocian, D. F.; Kirmaier, C.; Holten, D.; Mančal, T.; Ogilvie, J. P. Hidden vibronic and excitonic structure and vibronic coherence transfer in the bacterial reaction center. *Sci. Adv.* **2022**, *8* (1), eabk0953. DOI: 10.1126/sciadv.abk0953.
(18) Christensson, N.; Kauffmann, H. F.; Pullerits, T. n.; Mančal, T. s. Origin of Long-Lived Coherences in Light-Harvesting Complexes. *J. Phys. Chem. B* **2012**, *116* (25), 7449-7454. DOI: 10.1021/jp304649c.
(19) Wong, M. T.; Cheng, Y.-C. A quantum Langevin equation approach for two-dimensional electronic spectra of coupled vibrational and electronic dynamics. *J. Chem. Phys.* **2021**, *154* (15), 154107. DOI: 10.1063/5.0042848.
(20) Bennett, D. I. G.; Malý, P.; Kreisbeck, C.; Grondelle, R. v.; Aspuru-Guzik, A. n. Mechanistic Regimes of Vibronic Transport in a Heterodimer and the Design Principle of Incoherent Vibronic Transport in Phycobiliproteins. *J. Phys. Chem. Lett.* **2018**, *9* (10), 2665-2670. DOI: 10.1021/acs.jpclett.8b00844.
(21) Zhang, W. M.; Meier, T.; Chernyak, V.; Mukamel, S. Exciton-migration and three-pulse femtosecond optical spectroscopies of photosynthetic antenna complexes. *J. Chem. Phys.* **1998**, *108* (18), 7763-7774. DOI: 10.1063/1.476212.
(22) Yang, M.; Fleming, G. R. Influence of phonons on exciton transfer dynamics: comparison of the Redfield, Förster, and modified Redfield equations. *Chem. Phys.* **2002**, *282* (1), 163-180. DOI: 10.1016/s0301-0104(02)00604-3.
(23) Pachón, L. A.; Brumer, P. Computational methodologies and physical insights into electronic energy transfer in photosynthetic light-harvesting complexes. *Phys. Chem. Chem. Phys.* **2012**, *14* (29), 10094-10108. DOI: 10.1039/c2cp40815e.
(24) Novoderezhkin, V. I.; Doust, A. B.; Curutchet, C.; Scholes, G. D.; van Grondelle, R. Excitation Dynamics in Phycoerythrin 545: Modeling of Steady-State Spectra and Transient Absorption with Modified Redfield Theory. *Biophys. J.* **2010**, *99* (2), 344-352. DOI: 10.1016/j.bpj.2010.04.039.
(25) Irgen-Gioro, S.; Gururangan, K.; Spencer, A. P.; Harel, E. Non-Uniform Excited State Electronic-Vibrational Coupling of Pigment–Protein Complexes. *J. Phys. Chem. Lett.* **2020**, *11* (24), 10388-10395. DOI: 10.1021/acs.jpclett.0c02454.
(26) Nitzan, A.; Mukamel, S.; Jortner, J. Some features of vibrational relaxation of a diatomic molecule in a dense medium. *J. Chem. Phys.* **1974**, *60* (10), 3929-3934. DOI: 10.1063/1.1680840.

(27) Nitzan, A.; Jortner, J. Effects of vibrational relaxation on molecular electronic transitions. *J. Chem. Phys.* **1973**, *58* (6), 2412-2434. DOI: 10.1063/1.1679520.
(28) Silbey, R. Description of quantum effects in the condensed phase. *Procedia Chem.* **2011**, *3* (1), 188-197. DOI: 10.1016/j.proche.2011.08.026.
(29) Chen, X.; Silbey, R. J. Effect of correlation of local fluctuations on exciton coherence. *The Journal of Chemical Physics* **2010**, *132* (20), 204503. DOI: 10.1063/1.3435211.
(30) Kleinekathöfer, U. Non-Markovian theories based on a decomposition of the spectral density. *J. Chem. Phys.* **2004**, *121* (6), 2505. DOI: 10.1063/1.1770619.
(31) Meier, C.; Tannor, D. J. Non-Markovian evolution of the density operator in the presence of strong laser fields. *J. Chem. Phys.* **1999**, *111* (8), 3365-3376. DOI: 10.1063/1.479669.
(32) Garg, A.; Onuchic, J. N.; Ambegaokar, V. Effect of friction on electron transfer in biomolecules. *J. Chem. Phys.* **1985**, *83* (9), 4491-4503. DOI: 10.1063/1.449017.
(33) Womick, J. M.; Miller, S. A.; Moran, A. M. Toward the origin of exciton electronic structure in phycobiliproteins. *J. Chem. Phys.* **2010**, *133* (2), 024507. DOI: 10.1063/1.3457378.
(34) Hwang-Fu, Y.-H.; Chen, W.; Cheng, Y.-C. A coherent modified Redfield theory for excitation energy transfer in molecular aggregates. *Chem. Phys.* **2015**, *447*, 46-53. DOI: 10.1016/j.chemphys.2014.11.026.
(35) Chang, Y.; Cheng, Y.-C. On the accuracy of coherent modified Redfield theory in simulating excitation energy transfer dynamics. *J. Chem. Phys.* **2015**, *142* (3), 034109. DOI: 10.1063/1.4905721.
(36) Jang, S.; Cheng, Y.-C.; Reichman, D. R.; Eaves, J. D. Theory of coherent resonance energy transfer. *J. Chem. Phys.* **2008**, *129* (10), 101104. DOI: 10.1063/1.2977974.
(37) Bhattacharyya, P.; Fleming, G. R. The role of resonant nuclear modes in vibrationally assisted energy transport: The LHCII complex. *J. Chem. Phys.* **2020**, *153* (4), 044119. DOI: 10.1063/5.0012420.
(38) Lin, C.; Kim, T.; Schultz, J. D.; Young, R. M.; Wasielewski, M. R. Accelerating symmetry-breaking charge separation in a perylenediimide trimer through a vibronically coherent dimer intermediate. *Nat. Chem.* **2022**, *14* (7), 786-793. DOI: 10.1038/s41557-022-00927-y.
(39) Pandya, R.; Chen, R. Y. S.; Cheminal, A.; Thomas, T.; Thampi, A.; Tanoh, A.; Richter, J.; Shivanna, R.; Deschler, F.; Schnedermann, C.; et al. Observation of Vibronic-Coupling-Mediated Energy Transfer in Light-Harvesting Nanotubes Stabilized in a Solid-State Matrix. *J. Phys. Chem. Lett.* **2018**, *9* (18), 5604-5611. DOI: 10.1021/acs.jpclett.8b02325.
(40) Son, M.; Armstrong, Z. T.; Allen, R. T.; Dhavamani, A.; Arnold, M. S.; Zanni, M. T. Energy cascades in donor-acceptor exciton-polaritons observed by ultrafast two-dimensional white-light spectroscopy. *Nat Commun* **2022**, *13* (1), 7305. DOI: 10.1038/s41467-022-35046-2.
(41) Fidler, A. F.; Singh, V. P.; Long, P. D.; Dahlberg, P. D.; Engel, G. S. Dynamic localization of electronic excitation in photosynthetic complexes revealed with chiral two-dimensional spectroscopy. *Nat. Commun.* **2014**, *5* (1), 3286. DOI: 10.1038/ncomms4286.